

## Hysteresis Modeling, Identification and Fuzzy PID Control of SMA Wire Actuators Using Generalized Prandtl-Ishlinskii Model with Experimental Validation

Hamid Basaeri<sup>a</sup>, Mohammad Reza Zakerzadeh<sup>b\*</sup>, Aghil Yousefi-Koma<sup>c</sup>, Nafise Faridi Rad<sup>d</sup>, and Mohammad Mahdavian<sup>e</sup>

<sup>a</sup> Department of Mechanical Engineering, University of Utah, Salt Lake City, Utah, USA

<sup>b</sup> School of Mechanical Engineering, College of Engineering, University of Tehran, Tehran, Iran

<sup>c</sup> Center of Advanced Systems and Technologies (CAST), School of Mechanical Engineering, College of Engineering, University of Tehran, Tehran, Iran

<sup>d</sup> Department of Mechanical Engineering, University of British Columbia, Vancouver, British Columbia, Canada

<sup>e</sup> Department of Mechatronic Systems Engineering, Simon Fraser University, Surrey, British Columbia, Canada

---

### ARTICLE INFO

#### Article history:

Received: 20 Jun 2018

Accepted: 04 February 2019

#### Keywords:

Hysteresis Modeling

Fuzzy-PID Control

SMA Actuator

### ABSTRACT

In this paper, hysteretic behavior modeling, system identification and control of a mechanism that is actuated by shape memory alloy (SMA) wires are presented. The mechanism consists of two airfoil plates and the rotation angle between these plates can be changed by SMA wire actuators. This mechanism is used to identify the unknown parameters of a hysteresis model. Prandtl-Ishlinskii method is employed to model the hysteresis behavior of SMA actuators, and then, a self-tuning fuzzy-PID controller is designed based on the obtained model and implemented experimentally on the mechanism. The process of designing the controller has been implemented based on the model which results in compensating time and price. Self-tuning fuzzy-PID controller is applied to the closed control loop in order to control the position of the morphing wing. The performance of the controller has been investigated under different input signals including square and sinusoidal waves, and the results show the proper effectiveness of the method.

### 1. Introduction

Modeling and identification of Shape Memory Alloy (SMA) actuators for practical applications have attracted researchers due to some challenges. The chief difficulty in modeling and identification of these kinds of actuators is that they suffer from nonlinear saturated hysteretic behavior in forward and reverse transformation phases. Furthermore, there have been excessive challenges in controlling of SMA actuators during the recent years. Hysteresis behavior may result in steady state errors and limit cycle problems when conventional controllers are employed for trajectory control [1]. Furthermore, although feedback methods like Proportional-Integral (PI) control with appropriately tuned gains can provide adequate performance for slowly varying reference signals, they are not suitable for

oscillatory motions about the reference trajectory with fast varying reference signals [2].

In hysteresis, the value of the output of the system depends not only on the current input, but also on the previous inputs and/or the initial value. Actually, at any available point in the input-output diagram, there are several curves that may represent the future behavior of the system. The behavior of the curve is a function of the sequence of past maximum or minimum values of the input [3-6]. This kind of nonlinearity might cause performance degradation specifically in positioning applications. If this phenomenon is ignored, it will increase the inaccuracy in open loop control and degrades the tracking performance of the actuator [7]. Consequently, obtaining accurate mathematical models of these systems is a complex task [8-10]. Based on these

---

\* Corresponding author. Tel.: +98 21 611199620; e-mail: [zakerzadeh@ut.ac.ir](mailto:zakerzadeh@ut.ac.ir)

explanations, recent studies on control of SMA actuators have been led to use methods that are nonlinear.

There are numerous hysteresis mathematical models such as Preisach, Krasnosel'skii–Pokrovskii (KP), Prandtl–Ishlinskii (P-I), Duhem, Bouc–Wen, and Maxwell-Slip which are fully presented and analyzed according to their applications in modeling, control and identification of dynamical systems in Ref [7].

Preisach is one of the most popular operator-based models to predict the hysteresis behavior of nonlinear systems such as shape memory alloys [11] and magnetorheological fluids [12]. Duhem model, a rate-independent hysteresis model, was used for conducting polymer actuators by Wang et al. in Ref [13], and was experimentally identified and combined with the linear dynamics of the actuator. Also, the inversed form of the model was obtained and employed to control the displacement of the tri-layer actuators without having any external feedback. Identification process was carried out using an inverse neural network model. It was shown that the position tracking errors are diminished by more than 50% by integration of the hysteresis inverse model into an inversion-based feedforward controller.

In Ref [14], the application of a generalized play operator was investigated in formulating a generalized Prandtl–Ishlinskii (GPI) model. Their presented model can characterize symmetric and asymmetric hysteresis properties with output saturation. To describe asymmetric and saturated output–input hysteresis loops, the generalized play operator uses different envelope functions under increasing and decreasing inputs. The validity of their presented generalized model to characterize symmetric and asymmetric hysteresis properties was verified by comparing the model outputs with the measured major and minor hysteresis loops of various types of actuator such as SMA, magnetostrictive, and piezoceramic actuators. The modeling results show that the presented GPI model is capable of predicting the hysteresis loops of various smart actuators with the output saturation.

According to Sayyaadi et al. [15], the hysteresis of SMA actuators can efficiently be compensated by using the inverse of the phenomenological hysteresis models. In their work, the tip deflection of a large deflection flexible beam actuated by a SMA wire was controlled using a feedforward–feedback controller. The GPI inverse model was employed in feedforward part of the control system whereas a conventional proportional–integral (PI) feedback controller was added to the feedforward controller to improve the precision together with removing the steady state error in the process of position control. In another similar work, Zakerzadeh and Sayyaadi [16] used the GPI hysteresis model for modeling the hysteresis of SMA actuator. Using inverse of the GPI hysteresis model as a feedforward controller, they also implemented the position regulation control of the actuator. This work was carried out in a way that the proposed hysteresis model maps SMA temperature into position. To control the length of an SMA wire, different methods have been used. Due to hysteresis behavior of these materials, PID controllers are not appropriate solely [17]. Therefore, the combination of different controllers such as fuzzy and PID controller can be used. Ahn and Nguyen implemented this control method on SMA actuators [18]. Also, in [19–21], this technique has been implemented on different structures. Ahn and Nguyen implemented an optimized PID control method for SMA actuators by using genetic algorithm and the Preisach hysteresis model [17].

In the present research, it is experimentally shown that the GPI hysteresis model developed by Al Janaideh et al. in [14, 22–24] has a potent capability to predict hysteresis of SMA actuator. Also, the result of [25] demonstrates that amid the phenomenological hysteresis models such as Preisach model and Krasnosel'skii–Pokrovskii model, the GPI is capable of modeling the behavior of SMA actuators in a more accurate way. Additionally, the issue of tracking minor hysteresis loops because of considerable nonlinear behavior of the system has been addressed and studied in this paper since this problem has not been investigated in many papers. Furthermore, according to the result of our previous paper [26], rotation of a morphing wing mechanism has considerable sensitivity to the voltage that is applied to the SMA. Thus, in this work, the control tracking has been applied for a morphing wing mechanism actuated by one SMA wire. The main contribution of this work is to use P-I model and design a fuzzy controller based on this hysteresis model. The controller is designed using the identified P-I model and then is implemented on the experimental setup. In other words, only the model is used to design a controller without any need to have the experimental setup. This process of designing a controller would lead to saving much amount of time.

In this paper, first the GPI model developed by Al Janaideh et al. [22] is presented so as to predict the hysteresis behavior of a SMA wire actuator. After proposing the hysteresis model, an identification process based on Genetic Algorithm (GA) is presented. An optimization algorithm is also proposed in Section IV. GPI model is trained by some experimental data collected from a test setup consisting of a morphing wing mechanism actuated by SMA wire. The parameters of the GPI model are identified with the purpose of adapting the model response to the real hysteretic nonlinearity. The accuracy of the obtained GPI model with known parameters in modeling nonlinear hysteric behavior of first order ascending curves and higher order minor loops is validated. To verify the efficiency of the presented GA-based hysteresis model, a fuzzy-PID controller is implemented on closed-loop controller that uses a hysteresis model constructed from the proposed hysteresis model and some tracking control results are presented in Section VI. For square and sinusoidal waveform trajectories, the tracking control experiments are carried out. The results show small tracking errors in each case indicating proper identification of P-I model, and, designing a fuzzy-PID controller based on the model.

## 2. Generalized Prandtl–Ishlinskii Model

The classical P-I model characterizes the hysteretic behavior of materials using the classical stop (or play) operator with a density function. This operator is a continuous rate-dependent operator that determines the width of the hysteresis operator and is characterized by the input  $u$  and the threshold  $w$ . Further details about it can be found in [5, 27]. Assume that  $C_m[0, T]$  is the space of the piecewise monotone continuous functions and the input  $u(t) \in C_m[0, T]$  is monotone on each of the sub-intervals  $[t_i, t_{(i+1)}]$ , where  $t_0 < t_1 < \dots < t_i < t_{(i+1)} < \dots < t_N = T$ . So, the output of the generalized P-I model,  $y_{generalized}$ , can be derived as follows [14]:

$$y_{generalized}(t) = \int_0^w D(w) H_w[u](t) dw \quad (1)$$

where  $D(w)$  is an integrable positive density function,  $w$  represents the positive threshold as  $w_0 < w_1 < \dots < w_i < w_{(i+1)} < \dots < w_N = W$ , and  $H_w[u]$  is the generalized play hysteresis operator which can analytically be written as:

$$\begin{cases} H_w[u](0) = f_w(u(0), 0) \\ H_w[u](t) = f_w(u(t), H_w[u](t_i)) \end{cases} \quad (2)$$

where  $f_w(u, z) = \max\{\gamma_r(u) - r, \min(\gamma_r(u) - w, z)\}$ . For practical applications that use a finite number of generalized hysteresis play operators, Eq. (1) would be written as [14]:

$$y_{generalized}(k) = \sum_{i=0}^N D(w) H_{w_i}[u](k) \quad (3)$$

Based on Eqs. (1) and (3), the output of GPI model is a function of shape of the envelope, density and threshold functions. The hysteresis loop of a specific material generally defines the shapes of these functions. Moreover, whether such material has asymmetric hysteresis loops or not can affect the shape of these functions, and the output of these functions is a function of their parameters. Therefore, these parameters need to be obtained based on some experimental data of the actuator for properly modeling the behavior of these kinds of materials. Because of several appropriate properties of hyperbolic tangent functions [14], in this work, the following functions are chosen for the envelope functions of the generalized play operator:

$$\gamma_r(u) = P_1 \tanh(P_2 u + P_3) + P_4 \quad (4)$$

$$\gamma_l(u) = P_5 \tanh(P_6 u + P_7) + P_8 \quad (5)$$

Additionally, the density and threshold functions are selected as follows [14]:

$$p_k = P_9 e^{-P_{10} w_k} \quad (k = 0, 1, \dots, N) \quad (6)$$

$$w_k = P_{11} k \quad (k = 0, 1, \dots, N) \quad (7)$$

The 11 coefficients, including  $P_1, P_2, \dots, P_{11}$ , need to be identified for implementation of the GPI model. This process which is called training process can be carried out using input-output experimental data. In this work, the implementation of training process is accomplished with the MATLAB optimization Toolbox. The goal is to minimize the error between the predicted values from the P-I model and the values collected from experimental test setup. Experimental test setup with a SMA wire actuator is used to obtain the experimental data. The following section will explain more details about this experimental setup.

### 3. Morphing Wing Experimental Test Setup

Morphing wing is a wing capable of changing its shape at different flight conditions. As birds can change the shape of their wings in order to enhance flight performance, an aircraft wing can also have different shapes for different flight conditions. Therefore, there is a continues research to develop a wing capable of morphing like birds' wing, and several concepts and designs have been presented so far [28, 29]. Incorporating smart materials and structures into the design and fabrication of morphing wings, the interest in the morphing structures have been increased [30]. Shape memory alloy (SMA) actuators are one of the most common smart materials which are being used in these wings due to some their appropriate properties such as their high power to mass ratio, frictionless actuation, silence, and the simplicity of their mechanisms [31, 32].

The experimental setup that is used in this research consists of a mechanism which is suitable for applications related to

morphing wing which is shown in Figure 1. In other words, a wing can use this mechanism to change its shape at different flight conditions in order to increase its efficiency [33]. Universal joints are employed to connect SMA wire actuators to two airfoils allowing revolutions in two different directions. Two separate DOFs are achieved using two SMA wires, and the mechanism is capable of providing the sweep and gull degrees of freedom that are shown in Figure 2b and c respectively. Also, two springs are used causing the mechanism to come back to its initial position when the SMA actuators are not active since most of SMA actuators act in one direction (usually in tension).

Placing the mechanism between adjacent sections results in having large deformations and that would be a suitable design for morphing wing applications since it improves speed range and maneuverability of the aircraft. Gull and sweep modes can be achieved using this mechanism in a wing. Position sensors are embedded in the joints of the mechanism. Two directions of rotation can be generated independently using the SMA actuators. However, only one of these motions is used to prove the concept of the presented modeling strategy.

As shown in Figure 3, a morphing wing mechanism test setup and its components are used to study the ability of the GPI model in modeling the behavior of the presented mechanism actuated by a SMA wire. This test setup is also used to investigate the performance of control structure. Figure 4 shows the schematic interconnection of the experimental setup components. The setup which is used to obtain experimental data consists of a test-bed (the morphing wing mechanism actuated by SMA wire and a potentiometer), a PC with a Windows-based operating system, a data acquisition system, essential electronic circuits (bridge circuitry) and a DC power supply.

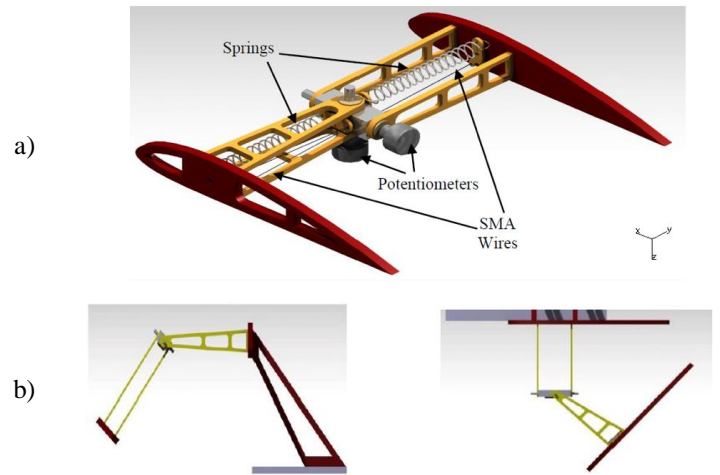
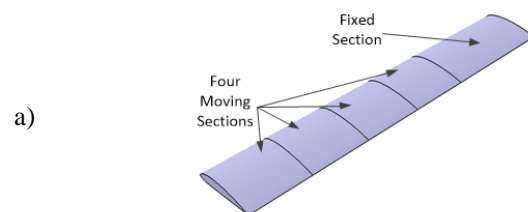


**Figure 1.** (a) Two degree of freedom SMA Actuated Morphing Mechanism, (b) Displaced shapes of the mechanism [26].



a)

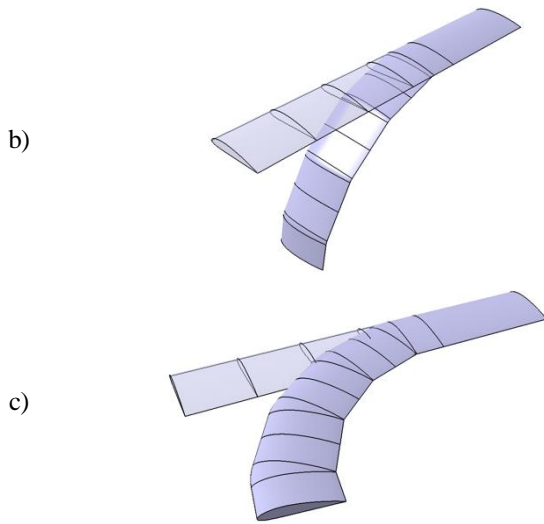


**Figure 2.** (a) Assemblage of different sections to achieve large deformations, (b) Deformed wing (gull), (c) Deformed wing (Sweep ) [26].

Table 1 presents the main specifications of the SMA wire actuator used in the proposed mechanism. The SMA actuator is made of Nitinol (Ni-Ti) alloy that has great electrical and mechanical properties, long fatigue life, and high corrosion resistance. The morphing wing mechanism is developed with a Flexinol actuator wire manufactured by Dynalloy Inc. This Ni-Ti SMA actuator wire is a one-way high temperature (90°C) shape memory with 0.01 inch diameter. Table 2 lists the specifications of the presented setup from that the experimental data is obtained to validate the results of P-I model as well as control system.

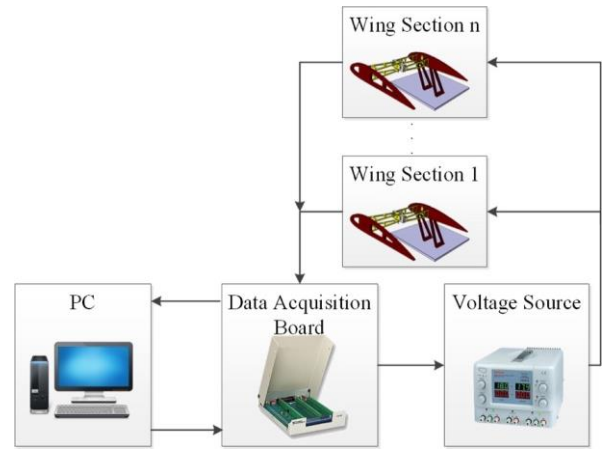


**Figure 4.** Schematic of the components of the experimental setup.

**Table 1.** SMA Specifications

Parameter	Definition	Value	Unit
$d_w$	Diameter	0.01	<i>In</i>
$\rho$	Density	6.45	<i>g/cm<sup>3</sup></i>
$M_f$	Martensite final temperature	43.9	<i>°C</i>
$M_s$	Martensite start temperature	48.4	<i>°C</i>
$A_f$	Austenite final temperature	68	<i>°C</i>
$A_s$	Austenite start temperature	73.75	<i>°C</i>

**Table 2.** Components of the Experimental Setup

Test-Bed	Morphing wing mechanism with 0.01-inch NiTi Flexinol wire & potentiometer pair, A test-stand
Data Acquisition	National Instrument, SCB-68 Noise Rejecting, Shielded I/O, Connector Block
PC	Hardware Core2 Duo 2 GHz CPU, 2GB RAM
	Software Windows 7, LabVIEW
Circuits	Bridge circuitry with instrumentation amplifying and anti-aliasing filter, Voltage-controlled current amplifier circuit

#### 4. Identification and Validation Processes

A slow decaying ramp signal shown in Figure 5 is the input to SMA wire. This input voltage is used to train the model and to identify the 11 unknown parameters of the GPI model. This input voltage is applied to the SMA wire and increases from a minimum value (i.e. zero) up to a value lower than maximum voltage and higher than some lower voltages which results to some First Order Descending (FOD) reversal curves attached to the ascending branch of the major loop. 642 data set containing

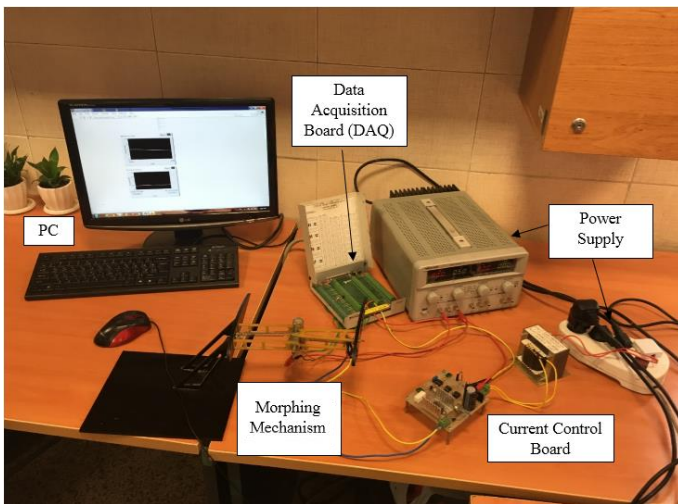


**Figure 3.** A View of the experimental test setup

the major loop and 10 first order descending reversal curves attached to the major loop is used for the training process of the GPI model. The switching values of these curves are chosen as: [3.5, 3.1, 3, 2.9, 2.8, 2.7, 2.6, 2.5, 2.4, 2.3, and 2.2] (volt). The input voltage to the current amplifiers of SMA actuator is illustrated in Figure 5. The change in the mechanism rotation is negligible for input voltage values less than 2.2 (volt). The experimental data used for the training process is shown in Figure 5(b).

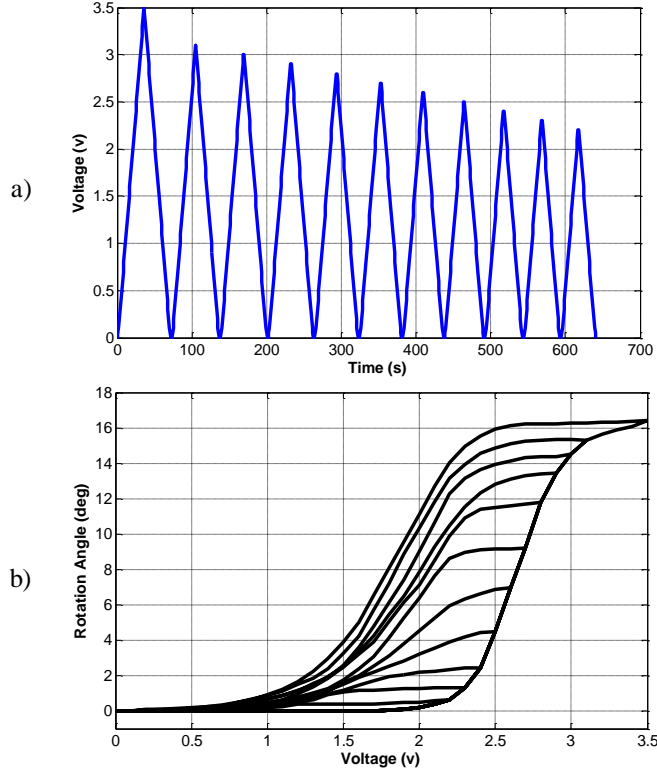


**Figure 5.** (a) Applied input voltage used for the training process, (b) Experimental data used for the training process.

The FOD curves have numerous advantages. For instance, compared to higher order transition curves, it is less hard to find FOD curves with experiments. Another advantage of FOD curves is that the measurements of these curves start from a well-defined state, namely the state of negative or positive saturation [5]. It is worthwhile to state that the input voltage is applied to the amplifiers of SMA actuators after the first cycle of SMA heating and cooling.

In this stage, an offline system identification problem should be solved. Unknown parameters of P-I model are considered as vector  $\Theta$ . A least-square loss function for the prediction-error is a natural minimization objective for system identification, stated as the following optimization problem:

$$\min_{\Theta} J(\Theta) = \sum_{k=1}^T (y_n^{\text{exp}}(t_k) - y_n^{\text{PI}}(x_a(t_k); \Theta))^2 \quad (8)$$

including the noisy experimental scalar measurement  $y_n^{\text{exp}}$  at the instant time  $t_k$  and its estimated value obtained through simulation. The simulation is implemented with unknown parameter values set to  $\Theta$ , assuming specific initial conditions for the states. In both the experiment and the simulation, a specific identification signal  $u$  which is depicted in Figure 5 is applied to the system as input.

There are many different ways to solve this optimization problem in hysteresis materials. Kao and Fung [34] utilized modified particle swarm optimization (MPSO) to identify the parameters of Scott–Russell mechanism which is driven by a piezoelectric element. A hysteresis modeling method that employs Genetic Algorithm (GA) was presented in [5] to obtain the optimized modeling parameters. Kwok et al. [35] suggested an asymmetric Bouc–Wen model for characterization of hysteresis in a magnetorheological fluid damper with the use of GA. A new genetic algorithm with adaptive crossover and mutation stage is developed to optimize the parameters of the model. Other techniques such as neuro-fuzzy [36–38] and particle swarm optimization [39] can also be used to identify the unknown parameters of the GPI model. In our study, GA is utilized for identification of the unknown parameters of P-I hysteresis model. The specifications of the GA implemented for the current system identification problem are listed in Table 3.

While motivated by targeting at the SMA-actuated morphing mechanism, the optimization problem formulated above, as well as all the solution methodology discussed hereafter in this section, applies to the comprehensive scope of nonlinear system identification. In gradient-based methods to this generic problem, gradients are obtained by numerically perturbing unknown quantities and measuring their effects on the prediction (modeling) error. This information is then used to find directions to search the design variables space. These approaches, although theoretically simple and extensively studied, can be very challenging and inefficient in practice [40]. Actually, handling the design constraints of the problem and the nonlinear hysteretic behavior of SMA might take substantial effort and the algorithms might easily get entrapped in local minima rather than converging to the global optimum. Extensive search, on the other hand, although having a great chance of convergence to the global minimum (provided that a fine grid is used to search the design space), is inefficient and mostly requires an excessive computational cost. To resolve these drawbacks, evolutionary algorithms exploit heuristics and soft-computing intelligence. Among these, the genetic algorithm (GA) has been chosen in this study due to its flexibility and benefits. Inspired by the way that nature selects better solutions and evolves its species, GA applies analogous concepts and mechanisms (including selection, crossover, mutation and elitism) to a population of solutions in order to evolve them and promisingly converge to a near global optimum. Genetic algorithms are well-established in the literature. More details on GA operators and concepts of their implementation, and some applications in engineering problems can be found in [41]. The whole process which is used in the identification process can be observed in Figure 6.

To identify the 11 unknown parameters of the GPI model, MATLAB optimization Toolbox is used. The identification process is implemented for minimizing the error between predicted output of the GPI model and the data obtained from the experimental test setup. The values of identified parameters are reported in Table 4. The P-I model, unlike other hysteresis modeling strategies, does not have exact output even for the training data. Therefore, Figure 7 compares the experimental data and the output of the GPI model for the actuation voltage input of Figure 5. According to this figure, the GPI model with selected envelope, threshold, and density functions with their identified parameters in Table 4 is capable of effectively characterizing the behavior of the SMA wire actuator. Of course, there are only some minor differences for some data. To show the accuracy of modeling in a better way, the maximum, mean and mean squared values of the absolute error are reported in Table 5. As the maximum rotation angle of the setup achieved by the SMA wire

actuation is 16.3 degree, the maximum modeling error in this case is about 9.33% of the maximum output. Additionally, the number of the generalized play operators, i.e. N, which was used in the modeling process, is chosen as 20.

**Table 3.** Specifications of the GA Implemented for System Identification

GA/Operation options	Value/Setting
Population Size	15
Generations	50
Selection	Type Stochastic uniform
	Fitness Ranking based on $J(\theta)$
Cross-over	Type Scattered
	Prob. 0.05
Mutation Prob.	0.05
Migration Fraction	0.2
Elite Count	2

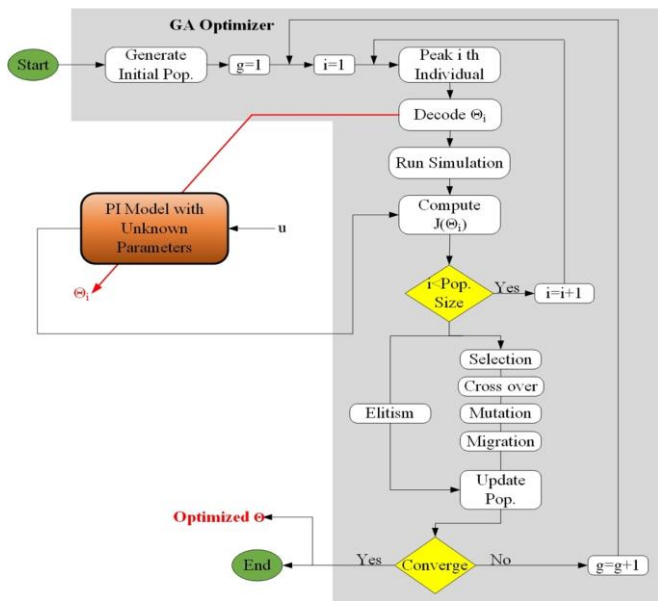


**Figure 6.** System identification process by GA

**Table 4.** Parameters of GPI Model Identified by GA

$P_1$	3.3784	$P_2$	1.6268	$P_3$	-3.7776
$P_4$	1.5592	$P_5$	3.7571	$P_6$	1.7893
$P_7$	-4.090	$P_8$	-1.154	$P_9$	0.5657
$P_{10}$	0.3016	$P_{11}$	0.1378		

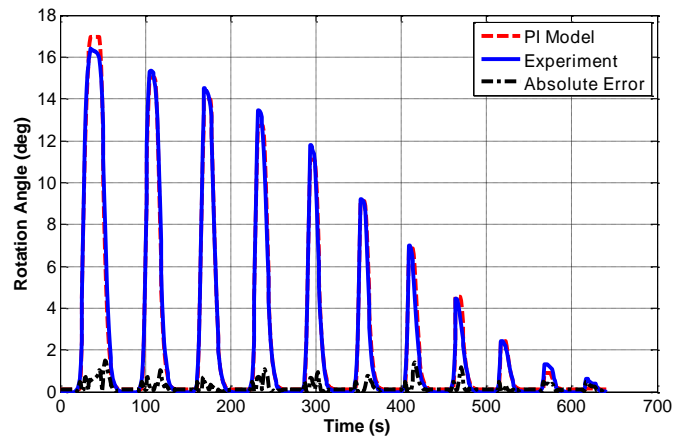
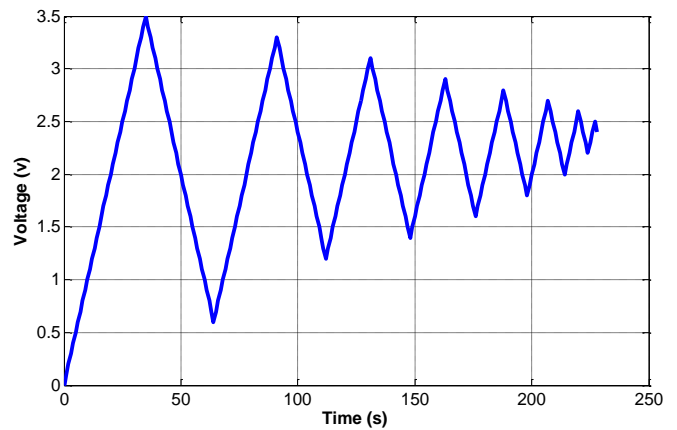


**Figure 7.** Comparison between the rotations of the mechanism predicted by the GPI model and the experimental test data - training process

**Table 5.** System Modeling Error - Training Process

Mean of Absolute Error	Max of Absolute Error	Mean of Squared Error
0.21 deg	1.52 deg	0.11 deg

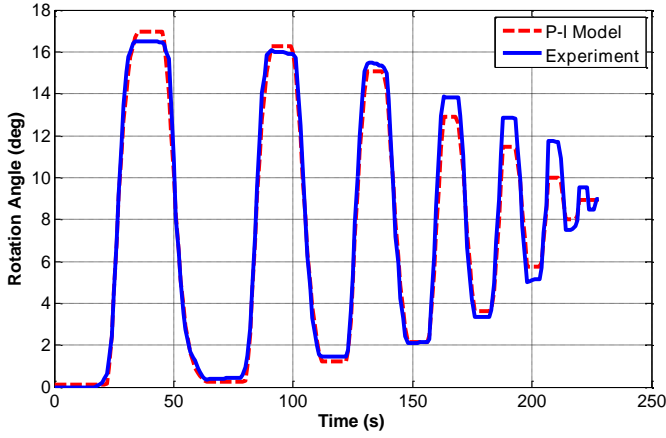
Majority of the current phenomenological hysteresis models have difficulty in modeling higher order hysteresis minor loops. For appraising the capability of GPI model in these situations, as the validation process, an input voltage profile shown in Figure 8 is used to actuate the SMA actuator.



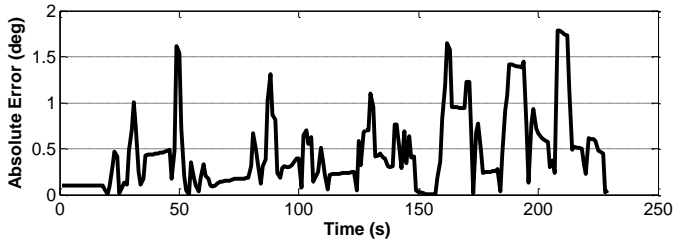
**Figure 8.** The input voltage applied in the validation process

Figure 9 shows the comparison between the prediction of the higher order hysteresis minor loops by the presented GPI model and the data obtained from the experimental setup. Figure 10 depicts the absolute error of the modeling process in time domain. Furthermore, Table 6 gives maximum, mean and mean square values of the absolute error.

According to Figure 9 and Table 6, the GPI model has acceptable accuracy in modeling and predicting the higher order hysteresis minor loops mainly in cases that it has been only trained with some first order hysteresis reversal curves attached to the major loop.



**Figure 9.** Comparison between the rotations of the mechanism predicted by the GPI model and the experimental test data in the validation process



**Figure 10.** Absolute error between the output of GPI model and experimental test data - validation process

**Table 6.** System Modeling Error - Validation Process

Mean of Absolute Error	Max of Absolute Error	Mean of Squared Error
0.46 deg	1.79 deg	0.38 deg

### 5. Fuzzy-PID controller

The control strategy for nonlinear hysteresis systems has been reported in literature for extensive ranges of application from piezoelectric actuators, micro-sliding friction, magnetorheological and magnetic damper, nanopositioning systems, SMA wires to medical devices with tendon-sheath mechanisms [15]. Altogether, one can classify two main approaches for such compensator, namely (i) open-loop control with no feedback from the output and (ii) close-loop control with availability of output feedback. In the second method, feedback signal clears out the error between the input and output signals and system's behavior remains unaffected to the external noises; Because of this reason, in this paper, a close-loop controller with angular position feedback is used.

In order to control the position of the morphing wing, self-tuning Fuzzy-PID controller is implemented on the SMA wire actuator. The nonlinear hysteresis behavior in smart actuators like the current mechanism may cause differences and difficulties while controlling a same test-bed in different environmental conditions. Therefore, in the systems with hysteresis behavior, PID controllers can only be used for a specific situation. Changing the environmental or initial condition or goal position

would cause a problem if the PID gains remain constant while these gains can be tuned using Fuzzy method. Using fuzzy rules, PID controller gains would be determined based on system behavior and error value.

#### 5.1. Fuzzy – PID structure

There are two different methods for defining a Fuzzy-PID controller and both methods contain two different layers. In the first method, a fuzzy controller is the first layer and a PID controller acts as a supervisor in the second layer. In the second method, the method used in the current study, PID controller acts as the main controller and the fuzzy controller is the supervisor. In this method, PID parameters are tuned using the fuzzy controller. By considering error and derivative of error values, the fuzzy controller selects appropriate values for PID gains, so by this self-tuning fuzzy PID controller, morphing wing mechanism can have adaptable behavior to different input signals. In this method, PID parameters are tuned using the fuzzy controller. Using a two-layered controlling method can increase stability and improve performance of the controller. The schematic structure of the second method which has been used in this paper can be seen in Figure 11.

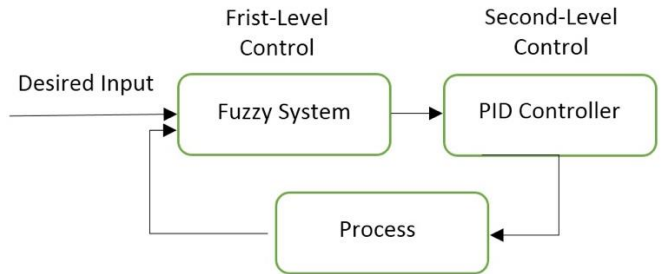


**Figure 11.** The schematic structure of the PID-fuzzy controller used in the current study

In order to calculate the controller parameters, first  $K_{pMin}$ ,  $K_{pMax}$ ,  $K_{dMax}$ , and  $K_{dMin}$  should be determined such that  $K_p \in [K_{pMin}, K_{pMax}]$  and  $K_d \in [K_{dMin}, K_{dMax}]$ . In order to simplify the procedure,  $K_p$  and  $K_d$  need to be normalized to [0,1] range using Eq.(9). Three parameters  $a$ ,  $K_{pp}$ , and  $K_{dd}$  are being calculated by the fuzzy system. Therefore, PID gains would be obtained by Eq.(9) and Eq.(10).

$$K_{jj} = \frac{K_j - K_{jMin}}{K_{jMax} - K_{jMin}} \quad j = p, d \quad (9)$$

$$K_i = K_p^2 / (aK_d) \quad (10)$$

Finally, the output of the fuzzy-PID controller is computed by using a classic PID controller mapping equation as follows:

$$G(s) = K_p + \frac{K_i}{s} + (sK_d) \quad (11)$$

The required maximum and minimum values for each gain can be seen in Table 7. It is noteworthy to mention that the designing process of the fuzzy-PID controller, i.e. evaluating controller parameters and choosing membership functions, is accomplished in simulation environment in MATLAB using P-I model presented in the paper. In the next step, all controller parameters are tuned by implementing the controller to the experimental setup. All the parameters in Table 7 are obtained by trial and error process in the simulation and optimization in the experimental tests.

**Table 7.** The Requested Maximum and Minimum for  $K_p$  and  $K_d$

	$K_d$	
	Min	Max
$K_p$	0.5	2
$K_d$	0	0.01

5.2. Fuzzifying the fuzzy controller inputs

The inputs of fuzzy controller are error and its derivative. The inputs need to be defined in fuzzy structure. Therefore, 7 triangular membership functions have been considered for each input. Five membership functions namely negative big (NB), negative medium (NM), negative small (NS), zero (ZE), positive small (PS), positive medium (PM) and positive big (PB) are used for inputs and outputs. The error and error's derivative membership functions can be seen in Figure 12.

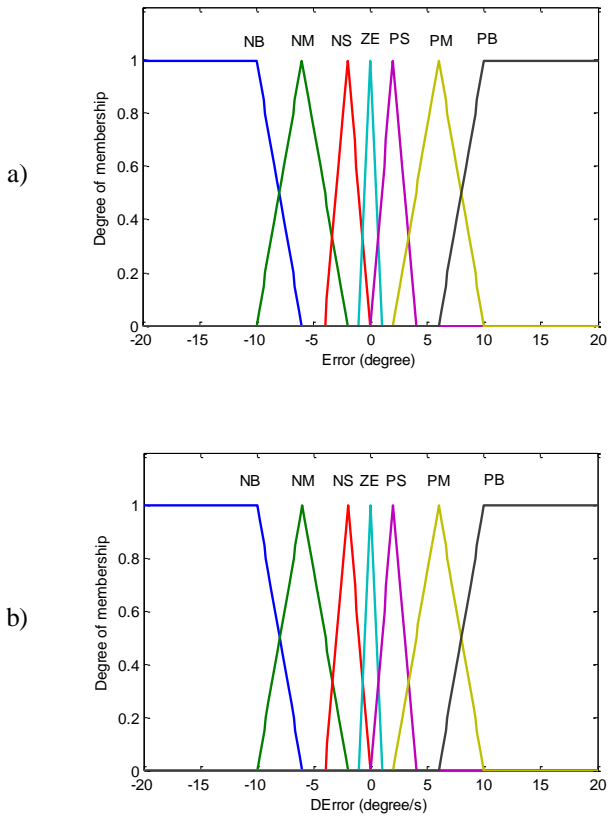


**Figure 12.** (a) Membership function for the error, (b) Membership function for the derivative of error

It should be notified that the error and error's derivative range are considered experimentally based on system behavior.

5.3. Defuzzifying the fuzzy controller outputs

The fuzzy controller's outputs are normalized PID parameters,  $K_{pp}$ ,  $K_{dd}$  and  $a$ . For each output, several triangular membership functions have been considered. Also, membership function type and amplitude have been considered experimentally. Figure 13 shows membership functions for fuzzy output of  $K_{dd}$ ,  $K_{dd}$ , and  $a$ .

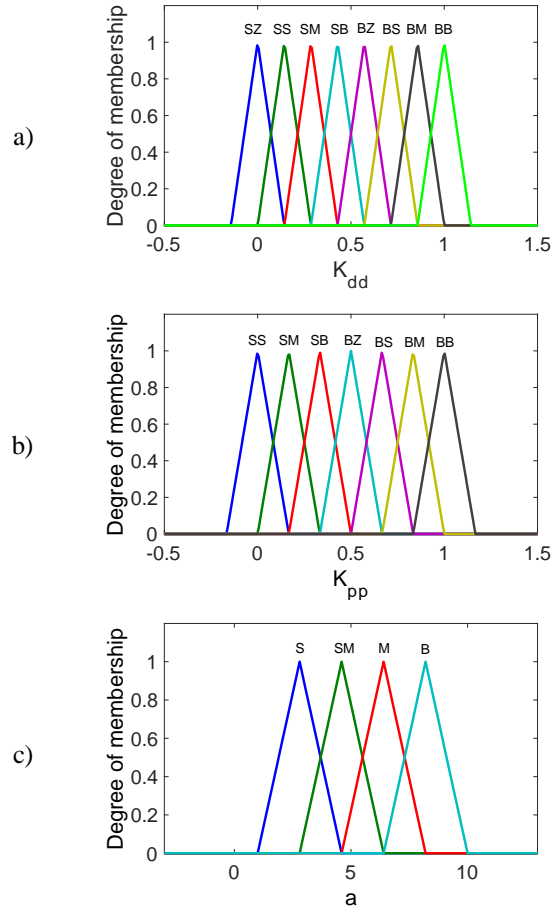


**Figure 13.** (a) Fuzzy output membership function for  $K_{dd}$ , (b) Fuzzy output membership function for  $K_{pp}$ , (c) Fuzzy output membership function for  $a$ .

5.4. Fuzzy rules

In order to use fuzzy controller properly, the following rules have been considered in Tables 8 to 10. It should be noticed that these rules have been chosen considering PID controller behavior and non-linear behavior of SMA wire in the simulation environment and using the GPI model.

**Table 8.**  $K_p$  Related Fuzzy Rules

e	ed	NB	NM	NS	ZE	PS	PM	PB
NB	BZ	BS	BM	BB	BM	BS	BZ	
NM	SB	BZ	BS	BM	BS	BZ	SB	
NS	SM	SB	BZ	BS	BZ	SB	SM	
ZE	SS	SM	SB	BZ	SB	SM	SS	
PS	SM	SB	BZ	BS	BZ	SB	SM	
PM	SB	BZ	BS	BM	BS	BZ	SB	
PB	BZ	BS	BM	BB	BM	BS	BZ	

**Table 9.**  $K_d$  Related Fuzzy Rules

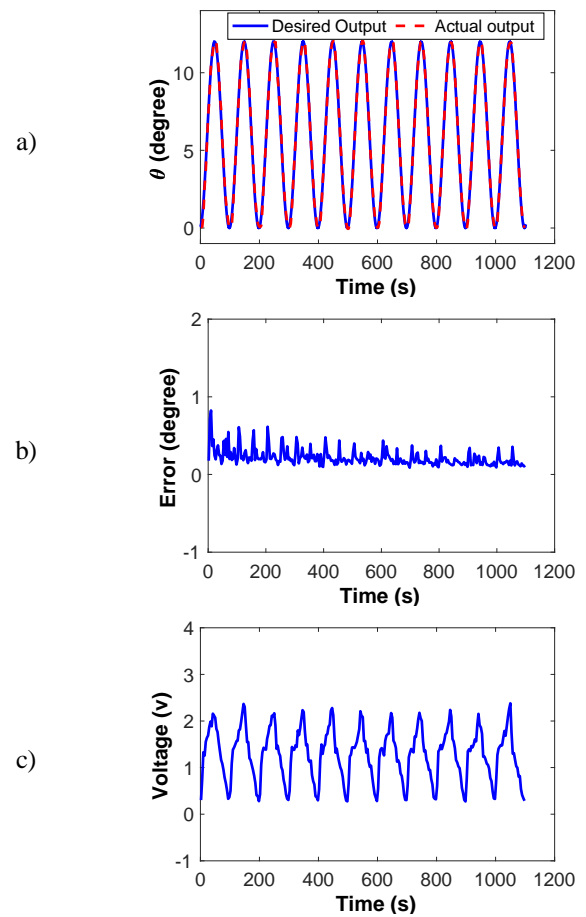
e	ed	NB	NM	NS	ZE	PS	PM	PB
NB	SB	SM	SS	SZ	SS	SM	SB	
NM	BS	BZ	SB	SM	SB	BZ	BS	
NS	BM	BS	BZ	SB	BZ	BS	BM	
ZE	BB	BM	BS	BZ	BS	BM	BB	
PS	BM	BS	BZ	SB	BZ	BS	BM	
PM	BS	BZ	SB	SM	SB	BZ	BS	
PB	SB	SM	SS	SZ	SS	SM	SB	

**Table 10.** “A” Related Fuzzy Rules

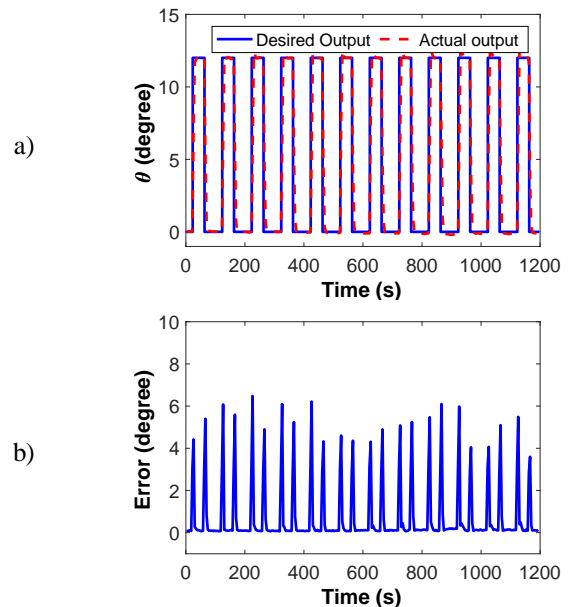
e	ed	NB	NM	NS	ZE	PS	PM	PB
NB	S	S	S	S	S	S	S	S
NM	MS	MS	S	S	S	MS	MS	
NS	M	MS	MS	S	MS	MS	M	
ZE	B	M	MS	MS	MS	M	B	
PS	M	MS	MS	S	MS	MS	M	
PM	MS	MS	S	S	S	MS	MS	
PB	S	S	S	S	S	S	S	

**6. Results and Discussions**

In this section, an experimental test is implemented to evaluate the performance of the fuzzy PID controller by applying three traditional signals to the system. Figure 14(a) illustrates tracking performance of the controller for a repeated sinusoidal trajectory with a frequency of 0.01 Hz and amplitude of 6 degrees. The absolute error between the desired and actual output of the system is presented in Figure 14(b). The error at the beginning of every period is due to inherent behavior of the system. Figure 14(c) shows the voltage that is applied to the system. Since the SMA wire used in the experimental setup has negligible strain in voltages under approximately 1.4 volts, after the controller exceeds this voltage, it can perfectly track the desired trajectory. Due to the slow response time of the SMA actuators, the controller performance is better in low frequencies.



**Figure 14.** Performance of the control system in tracking a sinusoidal reference command with a fixed amplitude: (a) Tracking control, (b) Absolute of tracking error (c) Applied voltage to the amplifiers of SMA actuators.



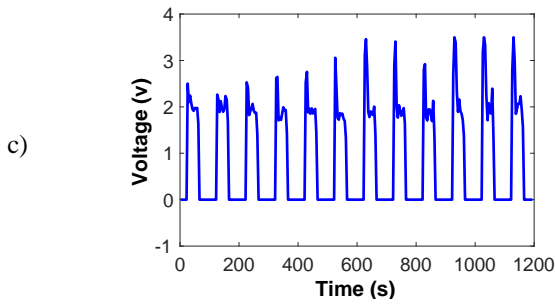


**Figure 15.** Performance of the control system in tracking a step input with a fixed amplitude: (a) Tracking control, (b) Absolute of tracking error (c) Applied voltage to the amplifiers of SMA actuators

Figure 15(a) shows the tracking performance of the controller for a repeated step trajectory with amplitude of 12 degrees. As can be seen from Figure 15(b), the steady state error is near zero. Applied voltage to the system is also illustrated in Figure 15(c). A decreasing sine wave is also applied as a command to the system to investigate the robustness of the fuzzy PID controller to different amplitudes as well as tracking minor hysteresis loops. Figure 16 represents the effectiveness of the controller regarding the mentioned problem.

In the tests with smooth inputs such as sinusoidal or decaying sinusoidal, angle changes occur gradually which is coincident with natural behavior of SMA wires. Therefore, suitable adaptation occurs during each cycle. However, in low voltages less accordance can be seen due to lower temperature of wires. Therefore, in the starting part of decaying sinusoidal period, bigger errors are obtained. On the other hand, an overshoot and bigger error may happen for the step inputs as a result of sudden changes in the voltage. In general, smooth inputs have more accurate and compatible response on SMA wires.

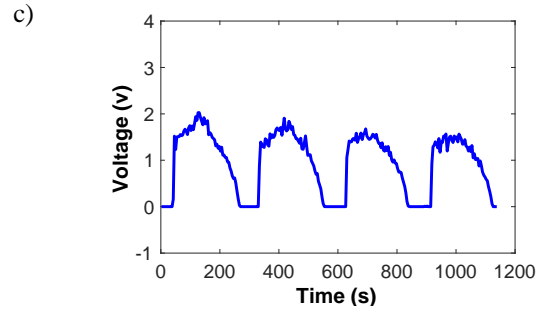
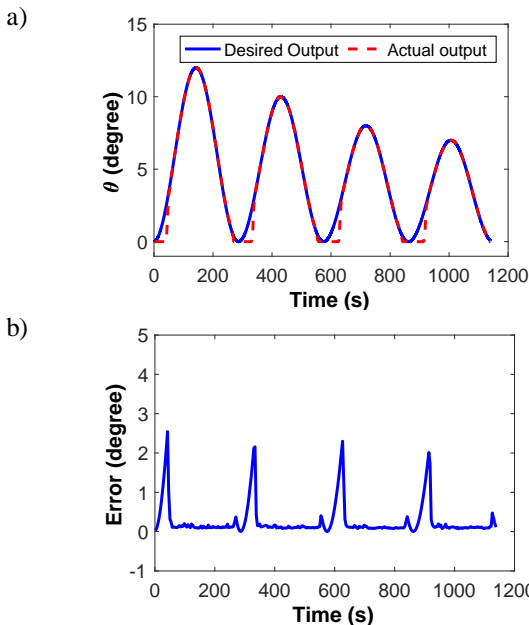


**Figure 16.** Performance of the control system in tracking a decaying sinusoidal command: (a)Tracking control, (b) Absolute of tracking error (c) Applied voltage to amplifiers of SMA actuators

## 7. Conclusion

In this work, a morphing wing mechanism actuated by shape memory alloy wires modeled by the generalized Prandtl–Ishlinskii model. The model was employed to predict asymmetric nonlinear hysteresis behavior of Shape Memory Alloy (SMA) actuator. Unknown parameters of the generalized Prandtl–Ishlinskii model were identified using the experimental data of the morphing wing mechanism. The identification process was done using a genetic algorithm and then the model was validated with a different set of experimental data. After validating the model, it was used as a plant in order to design a fuzzy-PID controller to control the presented mechanism actuated by a SMA actuator. The developed control system is capable of tracking square and sinusoidal trajectories with low tracking error. The presented control system can be implemented for other hysteresis materials due to the results of this work. Moreover, it is capable of being used in online applications, and results to appropriate tracking error for trajectory with hysteresis loops.

Furthermore, the control issue for SMA actuator was studied. The fuzzy-PID controller was developed and successfully applied to the real time position control of a SMA actuator. The controller was designed based on the P-I model. If there was not such a model, the process of designing a controller based on the experimental setup would be difficult. Based on the experimental results, the self-tuning fuzzy-PID controller was capable to adaptively achieve appropriate tracking for various references. Thus, the developed controller can be applied to a hysteresis system in order to improve the control performance and decrease the hysteresis effect of SMA actuators.

## Acknowledgments

The authors would like to thank Iran National Science Foundation (INSF) for their financial support.

## References

- [1] H. J. Lee, J. J. Lee, Time delay control of a shape memory alloy actuator, *Smart Materials and Structures*, Vol. 13, No. 1, pp. 227, 2004.
- [2] G. Webb, A. Kurdila, D. Lagoudas, Adaptive hysteresis model for model reference control with actuator hysteresis, *Journal of Guidance, Control, and Dynamics*, Vol. 23, No. 3, pp. 459-465, 2000.
- [3] X. Zhang, P. Feng, Y. He, T. Yu, Q. Sun, Experimental study on rate dependence of macroscopic domain and stress hysteresis

- in NiTi shape memory alloy strips, *International Journal of Mechanical Sciences*, Vol. 52, No. 12, pp. 1660-1670, 2010.
- [4] I. D. Mayergoyz, 2003, *Mathematical models of hysteresis and their applications*, Academic Press,
- [5] M. Brokate, J. Sprekels, 2012, *Hysteresis and phase transitions*, Springer Science & Business Media,
- [6] G.-L. She, F.-G. Yuan, Y.-R. Ren, H.-B. Liu, W.-S. J. C. S. Xiao, Nonlinear bending and vibration analysis of functionally graded porous tubes via a nonlocal strain gradient theory, Vol. 203, pp. 614-623, 2018.
- [7] V. Hassani, T. Tjahjowidodo, T. N. Do, A survey on hysteresis modeling, identification and control, *Mechanical systems and signal processing*, Vol. 49, No. 1-2, pp. 209-233, 2014.
- [8] C. LExcellent, H. Tobushi, Internal loops in pseudoelastic behaviour of Ti-Ni shape memory alloys: experiment and modelling, *Meccanica*, Vol. 30, No. 5, pp. 459-466, 1995.
- [9] D. Grandi, U. Stefanelli, A phenomenological model for microstructure-dependent inelasticity in shape-memory alloys, *Meccanica*, Vol. 49, No. 9, pp. 2265-2283, 2014.
- [10] A. Doroudchi, M. R. Zakerzadeh, M. Baghani, Developing a fast response SMA-actuated rotary actuator: modeling and experimental validation, *Meccanica*, Vol. 53, No. 1-2, pp. 305-317, 2018.
- [11] W. Raczka, J. Konieczny, M. Sibiak, J. Kowal, Discrete Preisach Model of a Shape Memory Alloy Actuator, *Solid State Phenomena*, Vol. 248, pp. 227, 2016.
- [12] S. Choi, Y. Han, Hysteretic behavior of a magnetorheological fluid: experimental identification, *Acta mechanica*, Vol. 180, No. 1-4, pp. 37-47, 2005.
- [13] X. Wang, G. Alici, X. Tan, Modeling and inverse feedforward control for conducting polymer actuators with hysteresis, *Smart materials and structures*, Vol. 23, No. 2, pp. 025015, 2013.
- [14] M. Al Janaideh, S. Rakheja, C.-Y. Su, A generalized Prandtl-Ishlinskii model for characterizing the hysteresis and saturation nonlinearities of smart actuators, *Smart Materials and Structures*, Vol. 18, No. 4, pp. 045001, 2009.
- [15] H. Sayyaadi, M. R. Zakerzadeh, Position control of shape memory alloy actuator based on the generalized Prandtl-Ishlinskii inverse model, *Mechatronics*, Vol. 22, No. 7, pp. 945-957, 2012.
- [16] M. R. Zakerzadeh, H. Sayyaadi, Precise position control of shape memory alloy actuator using inverse hysteresis model and model reference adaptive control system, *Mechatronics*, Vol. 23, No. 8, pp. 1150-1162, 2013.
- [17] G. Song, Robust position regulation of a shape memory alloy wire actuator, *Proceedings of the Institution of Mechanical Engineers, Part I: Journal of Systems and Control Engineering*, Vol. 216, No. 3, pp. 301-308, 2002.
- [18] N. B. Kha, K. K. Ahn, Position control of shape memory alloy actuators by using self tuning fuzzy PID controller, in *Proceeding of, IEEE*, pp. 1-5.
- [19] B. Kasemi, A. G. Muthalif, M. M. Rashid, S. Fathima, Fuzzy-PID controller for semi-active vibration control using magnetorheological fluid damper, *Procedia Engineering*, Vol. 41, pp. 1221-1227, 2012.
- [20] B. K. Sahu, T. K. Pati, J. R. Nayak, S. Panda, S. K. Kar, A novel hybrid LUS-TLBO optimized fuzzy-PID controller for load frequency control of multi-source power system, *International Journal of Electrical Power & Energy Systems*, Vol. 74, pp. 58-69, 2016.
- [21] R. K. Sahu, S. Panda, P. C. Pradhan, Design and analysis of hybrid firefly algorithm-pattern search based fuzzy PID controller for LFC of multi area power systems, *International Journal of Electrical Power & Energy Systems*, Vol. 69, pp. 200-212, 2015.
- [22] M. Al Janaideh, S. Rakheja, C.-Y. Su, An analytical generalized Prandtl-Ishlinskii model inversion for hysteresis compensation in micropositioning control, *IEEE/ASME Transactions on mechatronics*, Vol. 16, No. 4, pp. 734-744, 2011.
- [23] M. Al Janaideh, C.-Y. Su, S. Rakheja, Development of the rate-dependent Prandtl-Ishlinskii model for smart actuators, *Smart Materials and Structures*, Vol. 17, No. 3, pp. 035026, 2008.
- [24] M. Al Janaideh, O. Aljanaideh, Further results on open-loop compensation of rate-dependent hysteresis in a magnetostrictive actuator with the Prandtl-Ishlinskii model, *Mechanical Systems and Signal Processing*, Vol. 104, pp. 835-850, 2018.
- [25] M. R. Zakerzadeh, H. Sayyaadi, Experimental comparison of some phenomenological hysteresis models in characterizing hysteresis behavior of shape memory alloy actuators, *Journal of intelligent material systems and structures*, Vol. 23, No. 12, pp. 1287-1309, 2012.
- [26] H. Basaeri, A. Yousefi-Koma, M. R. Zakerzadeh, S. S. Mohtasebi, Experimental study of a bio-inspired robotic morphing wing mechanism actuated by shape memory alloy wires, *Mechatronics*, Vol. 24, No. 8, pp. 1231-1241, 2014.
- [27] A. Falvo, F. Furgiuele, C. Maletta, Hysteresis modeling of two-way shape memory effect in NiTi alloys, *Meccanica*, Vol. 43, No. 2, pp. 165-172, 2008.
- [28] M. Hassanalian, A. Abdelkefi, M. Wei, S. Ziaei-Rad, A novel methodology for wing sizing of bio-inspired flapping wing micro air vehicles: theory and prototype, *Acta Mechanica*, Vol. 228, No. 3, pp. 1097-1113, 2017.
- [29] S. Barbarino, O. Bilgen, R. M. Ajaj, M. I. Friswell, D. J. Inman, A review of morphing aircraft, *Journal of intelligent material systems and structures*, Vol. 22, No. 9, pp. 823-877, 2011.
- [30] J. Sun, Q. Guan, Y. Liu, J. Leng, Morphing aircraft based on smart materials and structures: A state-of-the-art review, *Journal of Intelligent material systems and structures*, Vol. 27, No. 17, pp. 2289-2312, 2016.
- [31] S. Barbarino, E. S. Flores, R. M. Ajaj, I. Dayyani, M. I. Friswell, A review on shape memory alloys with applications to morphing aircraft, *Smart Materials and Structures*, Vol. 23, No. 6, pp. 063001, 2014.
- [32] A. Sofla, D. Elzey, H. Wadley, Shape morphing hinged truss structures, *Smart Materials and Structures*, Vol. 18, No. 6, pp. 065012, 2009.
- [33] H. Basaeri, A. Yousefi-Koma, M. Zakerzadeh, S. Mohtasebi, Development of a bio inspired 2 DOF morphing wing actuated by shape memory alloy, in *Proceeding of*, 9-10.
- [34] C.-C. Kao, R.-F. Fung, Using the modified PSO method to identify a Scott-Russell mechanism actuated by a piezoelectric

element, *Mechanical Systems and Signal Processing*, Vol. 23, No. 5, pp. 1652-1661, 2009.

[35] N. Kwok, Q. Ha, M. Nguyen, J. Li, B. Samali, Bouc–Wen model parameter identification for a MR fluid damper using computationally efficient GA, *ISA transactions*, Vol. 46, No. 2, pp. 167-179, 2007.

[36] A. Mozaffari, A. Fathi, N. L. Azad, Preferred design of recurrent neural network architecture using a multiobjective evolutionary algorithm with un-supervised information recruitment: a paradigm for modeling shape memory alloy actuators, *Meccanica*, Vol. 49, No. 6, pp. 1297-1326, 2014.

[37] N. F. Rad, A. Yousefi-Koma, R. Mirjalili, H. Basaeri, Hysteresis modeling of SMA in the tail of a bioinspired vehicle by ANFIS, in *Proceeding of, IEEE*, pp. 445-448.

[38] N. F. Rad, M. Ayati, H. Basaeri, A. Yousefi-Koma, F. Tajdari, M. Jokar, Hysteresis modeling for a shape memory alloy actuator using adaptive neuro-fuzzy inference system, in *Proceeding of, IEEE*, pp. 320-324.

[39] M. Jokar, M. Ayati, A. Yousefi-Koma, H. Basaeri, Experiment-based hysteresis identification of a shape memory alloy–embedded morphing mechanism via stretched particle swarm optimization algorithm, *Journal of Intelligent Material Systems and Structures*, Vol. 28, No. 19, pp. 2781-2792, 2017.

[40] L. Ljung, Perspectives on system identification, *Annual Reviews in Control*, Vol. 34, No. 1, pp. 1-12, 2010.

[41] D. E. Goldberg, J. H. Holland, Genetic algorithms and machine learning, *Machine learning*, Vol. 3, No. 2, pp. 95-99, 1988.